Nanopolar structure in $Sr_xBa_{1-x}Nb_2O_6$ single crystals tuned by Sr/Ba ratio and investigated by piezoelectric force microscopy

Vladimir V. Shvartsman* and Wolfgang Kleemann
Angewandte Physik, Universität Duisburg-Essen, D-47048 Duisburg, Germany

Tadeusz Łukasiewicz
Institute of Electronic Materials Technology, Pl-01-919 Warsaw, Poland

Jan Dec
Institute of Physics, University of Silesia, PL-40-007 Katowice, Poland

(Received 19 September 2007; published 20 February 2008)

Complex as-grown nanodomain patterns are studied with piezoresponse force microscopy in $Sr_xBa_{1-x}Nb_2O_6$ single crystals at variant Sr/Ba molar ratios, $0.4 \leqslant x \leqslant 0.75$. They reflect random-field Ising model (RFIM) ferroelectricity, which crosses over into relaxor behavior at increasing x. This is explained by an increase of the polar disorder within the open tungsten-bronze crystal structure giving rise to enhanced quenched random electric fields at simultaneous decrease of the ferroelectric ordering temperature. The strongly anisotropic domain shapes, their fractal properties and size distributions, and their metastable occurrence above the nominal Curie temperature are in accordance with predictions for the RFIM.

DOI: 10.1103/PhysRevB.77.054105 PACS number(s): 77.80.Dj, 77.80.−e, 07.79.Lh, 77.84.Dy

I. INTRODUCTION

Strontium barium niobate, $Sr_xBa_{1-x}Nb_2O_6$ (SBN), is considered as a promising material for various applications, in particular, those exploring its nonlinear optical properties.[1,2] SBN has a tetragonal tungsten-bronze-type structure described by the general formula AB_2O_6. On cooling a phase transition from a paraelectric $4/mmm$ state to a polar $4mm$ state occurs.[3] The spontaneous polarization is oriented parallel to the c axis. Since no optic soft mode was found for SBN,[4] it can be described by an order-disorder pesudospin model.[5] On increase of the Sr/Ba ratio a transformation from ferroelectric to relaxor behavior takes place. In SBN compositions with $x > 0.6$ typical relaxor features such as a broad frequency dependent peak of the dielectric permittivity, ε, versus temperature, T, and nonzero remanent polarization above the peak temperatures of $\varepsilon(T)$ (Ref. 6) are observed. It is believed that the origin of the relaxor behavior in SBN is due to quenched electric random fields (RFs) related to randomly distributed vacancies on A sites of the unfilled tungsten-bronze structure.[5,7] Among six available A-site positions only five are occupied by nature. RFs promote the formation of short-range ordered polar nanoregions (PNRs) below so-called Burns temperature, T_d, which is several hundred degrees higher than the peak temperatures of $\varepsilon(T)$.[8] It is supposed that SBN exemplifies the three-dimensional random-field Ising model (3D-RFIM) universality class.[5] In this case, contrary to canonical relaxors such as $PbMg_{1/3}Nb_{2/3}O_3$, a transition into a long-range ordered ground state is expected below the Curie temperature, T_C. In reality, however, due to extreme critical slowing-down the dynamic PNRs are expected to merely transform into a random-field controlled metastable domain state. In spite of the fact that SBN was discovered more than 40 years ago,[2] information on the as-grown polar states of these materials is still scarce.

Transmission electron microscopy (TEM) studies at room temperature, i.e., below the transition temperature, have revealed a hierarchy of domain structures: a network of ferroelectric domains on a 300 nm scale seems to contain ferroelastic microtwins on a 50 nm scale.[9] Viehland *et al.* reported on a strong shape anisotropy of the 180° domains.[10] Along the polar c axis they are sized more than 1 μm, while in the ab plane the width of the domains was found to be 100–300 nm in SBN50, 20 nm for SBN60, and 10 nm for SBN75. It was supposed that random frozen-in quadrupolar fields and short-range strain interaction due to unoccupied A-site positions break the translation invariance of the polarization in the ab plane, but not along the c direction. The peculiar shape anisotropy of the 180° domains in SBN gives rise to a huge anisotropy of the second harmonic light scattering as reported recently for SBN61 by Betzler and co-workers.[11,12]

180° domains of size ≈50–100 nm in the ab plane having fractal-like shapes were recently imaged by piezoresponse force microscopy (PFM) in SBN75 (Ref. 13) and Ce-doped SBN61.[14–17] In the latter case the polar structure was studied in the vicinity of the transition temperature, where a coexistence of large quasistatic 3D PNRs, small dynamic PNRs, and virtually two-dimensional paraelectric interfaces was found.[15,16] The domain structure below T_C was found to be metastable, but showing slow "aging" dynamics toward equilibrium.[17]

In the present paper we report on results of the PFM studies done on different SBN compositions, which show increasing relaxor behavior as the Sr/Ba ratio increases. Thus the crossover from RFIM to relaxor ferroelectric behavior becomes "visualized" in a finely tuned way. Pertinent dependencies of domain properties such as fractal dimension and size distribution exponent are explored and discussed within the framework of the RFIM.

TABLE I. Chemical composition of the investigated SBN single crystals.

Initial charge composition	Single crystal composition	Notation in the text
$Sr_{0.4}Ba_{0.6}Nb_2O_6$	$Sr_{0.41}Ba_{0.58}Nb_2O_{5.44}$	SBN40
$Sr_{0.5}Ba_{0.5}Nb_2O_6$,	$Sr_{0.51}Ba_{0.48}Nb_2O_{5.78}$	SBN50
$Sr_{0.61}Ba_{0.39}Nb_2O_6$	$Sr_{0.59}Ba_{0.37}Nb_2O_{6.14}$	SBN61
$Sr_{0.75}Ba_{0.25}Nb_2O_6$	$Sr_{0.72}Ba_{0.25}Nb_2O_{6.13}$	SBN75

II. EXPERIMENTAL DETAILS

$Sr_xBa_{1-x}Nb_2O_6$ (SBN), $x=0.4-0.75$, single crystals used in this study were grown by the Czochralski method. Details of the growing procedure can be found elsewhere.[18] It should be mentioned that the real chemical compositions of the studied single crystals as estimated by inductively coupled plasma-optical emission spectroscopy differ slightly from the initial charge compositions (Table I). Platelet-shaped samples were cut perpendicular (*c* cut) and parallel (*a* cut) to the polar *c* axis (crystallographic direction [001]). The thicknesses of the samples were 0.5 and 0.3 mm, respectively. Polar structures were studied by PFM using a specially adapted commercial atomic force microscope (Topometrix, Explorer). A detailed description of the PFM method is given elsewhere.[19] The vertical PFM mode, which is sensitive to an out-of-plane component of the polarization, was applied to the *c*-cut samples, while the *a*-cut samples were studied by the lateral PFM mode, which probes an in-plane component of the polarization. A commercial conductive tip-cantilever system NCHR (Nanosensors) with a spring constant of 40 N/m and tip apex radius of about 10 nm was used. Domain visualization was performed under an applied *ac* voltage with an amplitude $V_{ac}=5-10$ V and a frequency $f=15$ kHz. The probing frequency was chosen far away from resonant frequencies of the cantilever-sample-holder system to avoid ambiguity of the experimental data. A home made heater was used allowing us to measure in the temperature range 290–350 K.

III. EXPERIMENTAL RESULTS AND DISCUSSION

A. Polar structure at room temperature

Figure 1 shows the PFM images obtained on the *c*- and *a*-cut samples of ferroelectric SBN40. The images are presented in a trimodal false color code. The white and red colors correspond to domains with the spontaneous polarization oriented up and down relative to the figure plane (vertical PFM) and left and right in the figure plane (lateral PFM), respectively. The yellow contrast corresponds to regions with negligible piezoresponse. In the plane perpendicular to the polar axis we see a complex maze-type domain pattern. The domain boundaries are strongly jagged. Contrastingly, on the *a*-cut sample we find stripe domains extended along the polar axis. The domains are strongly anisotropic: they have typical sizes of about 0.5–1 μm perpendicular to polar axis, but several tens of microns along it. This observation is in good agreement with TEM data reported earlier.[10] A simple explanation of the observed shape anisotropy can be found under the assumption of a corresponding anisotropy of the inter- and intralayer interactions, J_c and J_a, acting between the ferroelectric O-Nb-O "spin" chains along the *c* and *a*(*b*) axes, respectively. Within the framework of an anisotropic Ising model we can consider the excess of the free energy for RF-induced domains[7] in a first approximation for a square column-shaped domain with length L_c (in lattice units) and cross section L_a^2 as

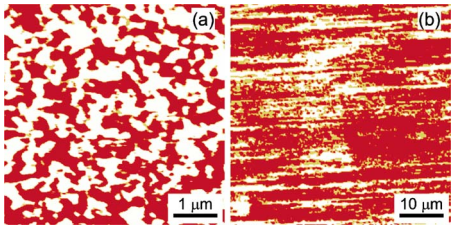

FIG. 1. (Color online) PFM images of the SBN40 single crystal observed on a *c*-cut sample in the vertical mode (a) and on an *ab* cut in the lateral mode (b).

$$W = 2L_a^2 J_c + 4L_a L_c J_a - hL_a\sqrt{L_c}, \quad (1)$$

where h is the average RF acting on the statistical excess $\sqrt{N}=\sqrt{L_a^2 L_c}$ of up (or down) spins.[7] Minimization of the free energy with respect to both L_a and L_c yields the relationship $L_a/L_c=J_a/J_c$. Hence, $L_a \ll L_c$ as observed experimentally seems to indicate the relationship $J_a \ll J_c$. In a more complete consideration of the domain stability also the effects of depolarization fields have to be taken into account. To this end one should take care of the condition $\mathrm{div}\, P \approx 0$ to be fulfilled at the domain boundaries for minimizing the domain wall energy.[20] For uniaxial ferroelectrics this means that domain walls perpendicular to polar axis are energetically unfavorable and the domains will have needlelike rather than square column shapes. This is an additional factor promoting the observed anisotropy of domain shape in SBN.

In Fig. 2 the PFM images acquired on *c*-cut single crystals with different Sr/Ba ratios are presented. All samples have been aged over about one year at room temperature, $T \approx 295$ K, before being scanned by PFM. This temperature lies below the peak temperature of the dielectric permittivity, T_m, for all of the specimens. They can, hence, be considered to be in quasistable final states, which nevertheless reflect the different initial subdivisions into differently sized domains by RFs of different strengths. One can see that the domains become smaller and their boundaries increasingly jagged in samples with higher Sr content. At the same time "yellow" regions take up a larger total area. We can attribute these piezoinactive areas either to very fine polar structures with size below 10 nm being unresolved under our experimental conditions, or to a paraelectric phase under short-range correlated ("quasistaggered") RFs.[15]

Figure 3(a) shows the domain-size distributions, $N_S(S)$ vs S, for the different SBN compositions. Here $N_s dS$ is the number of nanodomains within the range of areas $S \cdots S+dS$. One can see that even in the ferroelectric SBN40 the sizes of the

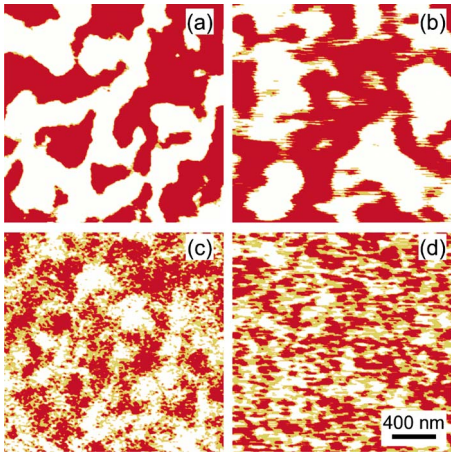

FIG. 2. (Color online) PFM images observed on a *c*-cut SBN single crystals with various compositions: SBN40 (a), SBN50 (b), SBN61 (c), and SBN75 (d).

domains, curve 1, are distributed in a broad range. On increasing the Sr/Ba molar ratio, $x=0.61$ (curve 2) and 0.75 (curve 3), the number of smaller domains increases, while large domains become rare. As a result, the mean domain size

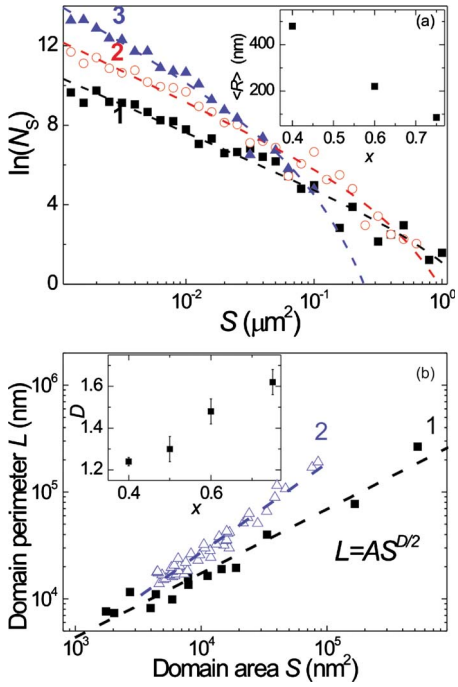

FIG. 3. (Color online) (a) Domain-size distributions measured at room temperature on single crystals of SBN40 (1), SBN61 (2), and SBN75 (3). The broken lines are best fits to Eq. (3). For the fit parameters, see Table II. The inset shows the dependence of the mean domain size $\langle R\rangle$ on the Sr concentration x. (b) Domain perimeter, L, versus area, S, for the determination of the fractal dimension, D, of the domain boundaries for the PFM images taken on SBN40 (1) and SBN75 (2) single crystals. The inset shows the concentration dependence, D vs x.

TABLE II. Parameters of the domain-size distributions obtained from the best fit of experimental data $N_S(S)$ [Fig. 3(a)] to Eq. (3).

	δ	S_0 (μm^2)
SBN40	1.2 ± 0.1	1.1 ± 0.1
SBN61	1.3 ± 0.1	0.7 ± 0.2
SBN75	1.6 ± 0.15	0.05 ± 0.02

$$\langle R\rangle = 2\sqrt{\pi^{-1}\int_0^\infty N_S S dS / \int_0^\infty N_S dS} \tag{2}$$

estimated from the $N_S(S)$ distributions decreases with increasing x [see inset to Fig. 3(a)]. For Ce-doped SBN it was reported previously that the domain-size distribution follows a power law with exponential cutoff[14]

$$N_S \sim S^{-\delta}\exp(-S/S_0), \tag{3}$$

where S_0 corresponds to a cutoff size, above which domains become rare. The same law describes the domain distributions quite well also in the present study. The best-fit parameters for different SBN compositions are listed in Table II. One can see that the value of the parameter S_0 in the "relaxor" SBN75 is almost 2 orders of magnitude smaller than in the "ferroelectric" SBN40. On the other hand, the value of the exponent δ increases with increasing x, $\delta(0.4)=1.2$, $\delta(0.61)=1.3$, and $\delta(0.75)=1.6$. It should be mentioned that the parameters obtained for SBN75 are comparable to those reported earlier for Ce-doped SBN61.[14] In that case the Ce doping enhances the relaxor behavior due to its excess ionic charge. Hence, the properties of the material should be close to the properties of the compositions with higher Sr content. We notice that the relaxor properties of SBN61 are obviously increased by about the same amount when doping with either 1.1% of Ce^{3+} (Ref. 14) or 14% of Sr^{2+} in exchange of Ba^{2+} (this paper). This sheds some light onto the strongly different RF activities of hetero- and isovalent doping in relaxors (see discussion below).

It is worth comparing the obtained experimental data with theoretical predictions for the RFIM systems. In particular, it was shown that the domain-size distributions are described by a power law with exponential cutoff in the case of two-dimensional RFIM systems.[21,22] While in our case the domain structure is in reality a 3D system, PFM probes a projection of this 3D domain pattern on a sample surface. This projection is actually a two-dimensional (2D) object and may be described by 2D RFIM statistics. In the 2D model both parameters, S_0 and δ, depend on the strength of the RFs.[21,22] Namely, S_0 decreases at increasing RFs, while the exponent δ approaches the value 1.55 in the limit of strong RFs. A similar tendency is now observed for the experimental domain-size distributions at increasing Sr/Ba ratio. Thus we can assume that the effect of the RFs becomes stronger in the composition with higher Sr content, i.e., in compositions showing more pronounced relaxor behavior.

The shape of the domains reminds of fractal-like objects similar as those found in Monte Carlo simulations of the RFIM systems.[23] Quantitatively the shape of the domain

walls may be analyzed by determining their fractal dimension. PFM images show cross sections of 2D domain walls within the sample surface. These cross sections, which we call domain boundaries, are one-dimensional objects, whose fractal dimension, D, may be estimated by analyzing a relationship between the area of individual domains, S, and their perimeter, L,[24]

$$L^{1/D}S^{-1/2} = \text{const.} \quad (4)$$

Figure 3(b) shows the experimental dependences, L vs S, which follow power laws according to Eq. (4) quite satisfactorily. The x dependence of the best-fitted values of D is shown in the inset to Fig. 3(b). One can see that the fractal dimension of domain walls increases at increasing Sr content. It is interesting to compare the experimental data with theoretical predictions. Theoretically determined fractal dimensions for the 2D RFIM have been reported to be $D=1.18$ using Monte Carlo simulations[23] and $D=1.96$ from the exact solution for the ground state.[22] The large difference between these two theoretical values is partly due to the large distance of the Monte Carlo simulations from thermal equilibrium. In addition, their small D value refers to rather weak RFs and to finite temperatures,[23] parameters both of which favor weak domain wall roughness, since local pinning can easily be overcome by thermal fluctuations. Our values $D(0.4)=1.23$, $D(0.5)=1.29$, $D(0.61)=1.48$, and $D(0.75)=1.60$ lie between these two theoretical values.

The increase of the fractal dimension D indicates that the polar disorder becomes increasingly pronounced at increasing Sr content. It is worth mentioning that even in ferroelectric SBN40 the domains are considerably less regular in comparison to those observed in other uniaxial ferroelectrics such as triglycine sulphate.[25] While the domains in SBN40 look more compact than in other SBN compositions, the fractal dimension of their boundaries clearly differs from $D=1$ as expected for completely compact domains. This fact confirms our conjecture that the generic vacancy distribution of the open tungsten structure relates SBN40 to the case of RFs, which pin and distort domain walls to form a metastable pattern even after an aging time of one year at room temperature.

Indeed, the primary sources of RFs are the same in all SBN compounds, irrespective of their Sr/Ba molar ratio. As was already mentioned, the SBN single crystals have natural A-site vacancies, which are sources of inherent charge disorder. They are distributed among two kinds of A sites, two 12-fold coordinated $A1$ sites, which are otherwise occupied only by Sr cations, and four 15-fold coordinated $A2$ sites, which otherwise host both Sr^{2+} and Ba^{2+} ions.[26] Crystallographic studies have shown that the vacancy tends to increasingly occupy the $A2$ sublattice as x increases. E.g., its distribution ratios between $A1$ and $A2$ sublattices are V_{A1}: $V_{A2} \approx 0.59:0.41$, 0.55–0.70:0.45–0.30, and 0.35:0.65 for $x=0.33$,[27] 0.61,[28] and 0.75,[26] respectively, where $V_{A1}+V_{A2}=1$.

Another source of disorder is the simultaneous occupation of $A2$ sites with Sr^{2+} and Ba^{2+} ions. This introduces disorder of the oxygen ion positions due to different Ba-O and Sr-O binding lengths.[26] Accommodation misfits of the different oxygen octahedra give rise to local buckling and tilting deformations. Thus localized electric multipole moments are expected similarly as conjectured for isovalently substituted $BaTi_{1-x}Zr_xO_3$.[29] They are sources of random electric fields, which add to the charge-induced ones. Their efficiency can be estimated by considering the mixing entropy $k_B \ln W$, where W is the number of ways of distributions of Sr and Ba ions as was calculated by Kim *et al.*[30] under the constraint of a constant vacancy distribution ratio V_{A1}: V_{A2}, where $V_{A1}+V_{A2}=1$. For the above occupation ratios a monotonic increase of S at increasing x occurs within $0.3<x<0.7$, becoming virtually constant within $0.6<x<0.7$.

In order to understand the observed growing tendency of disorder, viz., relaxor properties, for Sr^{2+} contents above $x=0.6$ one should recall that the missing charges on the vacancies are the most intense sources of RFs. They exert shifts of Nb^{5+} cations from their central positions in the NbO_6 octahedra. Assuming only nearest neighbor interaction it is easily seen that $A1$-site vacancies have no influence on 1/5 of the NbO_6 octahedra, viz., those sitting on $B1$ (edge) sites. Since an increase of the Sr^{2+} content results in a vacancy redistribution from $A1$ to $A2$ sites, the corresponding "active" charge disorder will be enhanced at large Sr^{2+} content.

The above consideration shows that SBN40 is subject to minimum mixing disorder. It is, hence, the system with the weakest RFs, which obviously still shows typical ferroelectric behavior. Its RFIM properties, in particular, the unusual critical behavior,[7] still remain to be shown. As the Sr^{2+} content increases both the disorder and charge-induced RFs become stronger. They give rise to the observed downward shift of the transition temperature in accordance with the expected RF crossover.[31] At a certain Sr/Ba substitution level, $x \geq 0.6$, the effect of the RFs becomes dominant and a transformation into typical relaxor behavior takes place. A similar fine-tuning of the magnitude of the RFs is observed, e.g., in isovalently substituted $BaTi_{1-x}Sn_xO_3$, where Sn doping levels as high as $x \approx 0.25$ are necessary to drive the system from a pure ferroelectric via a RF-perturbed one into the relaxor state.[32]

B. Temperature evolution of polar structures

We have investigated the temperature evolution of the domain patterns in SBN61 and SBN75 single crystals in the vicinity of their phase transitions. In the compositions with lower Sr^{2+} concentrations the Curie temperature regions were unfortunately not accessible under our experimental conditions. The results are in good agreement with those reported earlier for Ce^{3+}-doped SBN61.[15,16] Namely, relatively large quasistatic regions of correlated piezoresponse (with size ≈ 100 nm) are observed above the nominal Curie temperatures, $T_C \approx 346$ K (Ref. 7) and ≈ 300 K,[33] respectively (Fig. 4). The term "quasistatic" means here that the shape and the location of these regions do not change substantially during several consecutive scans, i.e., they are static on our experimental time scale, $t \approx 10^3$ s. It should be stressed that the domain patterns presented in Fig. 4 display aged situations both at room temperature (one year) and at elevated temperatures above the nominal transition (1 h). The results are, hence, not affected by arbitrary intermediate nonequilibrium situations.

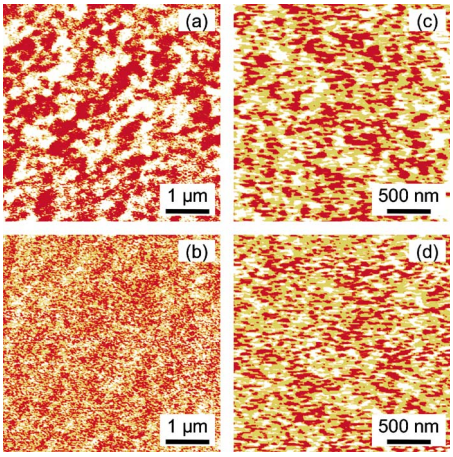

FIG. 4. (Color online) PFM images taken on a SBN61 single crystal [$T_C \approx 346$ K (Ref. 5)] at 295 (a) and 363 K (b) and on a SBN75 single crystal [$T_C \approx 300$ K (Ref. 33)] at 295 (c) and 313 K (d). Color codes are explained in the text.

Since the value of the piezoresponse signal is relatively small, the existence of regions of correlated piezoresponse (i.e., correlated polarization) was verified by an autocorrelation function analysis. Such procedure was successfully applied in previous studies of complex nanodomain structures in relaxors.[34,35] Autocorrelation images [Fig. 5(c)] were obtained from the original PFM images by the following transformation:

$$C(r_1,r_2) = \sum_{x,y} D(x,y)D(x+r_1,y+r_2), \tag{5}$$

where $D(x,y)$ is the value of the piezoresponse signal. Positive or negative values of the autocorrelation function correspond to probabilities to find a region with parallel or antiparallel direction of the polarization after a shift on (r_1,r_2) from an arbitrary point in the original PFM image. Typically, a peak arises in the center of the autocorrelation images. For the paraelectric state, in the absence of piezoactive regions, the width of the "central" peak is determined by the resolution of the PFM image as well as by scan parameters (scanning velocity, probing frequency, and time constant of the lock-in amplifier). The condition that the width of the central peak in the autocorrelation image becomes larger than the minimal size related to noise was used as a criterion of appearance of a region of correlated polarization. Both in the SBN61 and SBN75 it occurs approximately 15 K above the corresponding transition temperature [Fig. 5(c), curves 1 and 2].

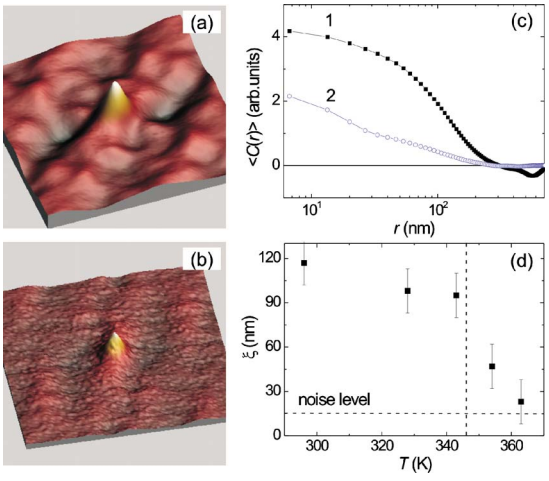

FIG. 5. (Color online) Autocorrelation images taken on SBN61 at 295 (a) and 354 K (b). (c) Distance dependence of the autocorrelation function, $\langle C(r)\rangle$, averaged over all in-plane directions for SBN61 at 295 (1) and 354 K (2). (d) Temperature dependence of the mean correlation radius ξ of SBN61.

In order to estimate the mean size of these regions we averaged the autocorrelation image over all in-plane directions and then approximate it by the relation

$$\langle C(r)\rangle = \sigma^2 \exp[-(r/\langle\xi\rangle)^{2h}]. \tag{6}$$

Here $\langle\xi\rangle$ is a mean correlation length. It is worth mentioning that contrary to observations in the perovskite relaxor PMN-PT[35] only short-range correlations describing individual PNRs were found in SBN. No long-range correlations related to a preferential orientation of PNR interfaces along certain crystallographic directions were observed. Figure 5(d) shows the temperature dependence of $\langle\xi\rangle$ for SBN61. Lacking intermediate equilibration it has to be understood as a transient curve. It decreases monotonically with increasing temperature up to T_C, and then abruptly vanishes above T_C. Nevertheless at $T \approx T_C + 15$ K the value of $\langle\xi\rangle$ is still not yet negligible.

We attribute the regions of correlated polarization observed above T_C to mesoscale PNRs, which grow in the vicinity of the phase transition and become immobilized on our time scale due to their large size. A detailed discussion of this phenomenon can be found elsewhere.[15] Here we would like to mention that the occurrence of quasistatic PNRs above the transition temperature supplements the present point of view on a transformation from ergodic relaxor into either nonergodic relaxor or ferroelectric behavior. It shows that this transformation is continuous, rather than abrupt. In a certain temperature range above T_C the system contains both small dynamic and large quasistatic PNRs. The latter ones are precursors of domains in the low-temperature ferroelectric state. The nonergodic character of such a system was verified by the observation of aging of the dielectric susceptibility,[15] which is probably related to isothermal growth of quastistatic PNRs at the expense of the dynamic ones.

While quasistatic PNRs are not detectable above $T_C + 15$ K, a nonzero piezoresponse may be induced even at higher temperatures after applying an external electric field. Figure 6 shows the local piezoresponse hysteresis loops measured in SBN75 at different temperatures. In this experiment the tip was stopped at a certain location, and a sequence of voltage pulses was applied with the amplitude cycling from $-V_{max}$ to V_{max}. After each pulse the piezoresponse was measured. On heating both the maximum and the remanent (at zero *dc* voltage) values of piezoresponse are decreasing. Nevertheless a hysteresis is still observed at 350 K, which is higher than 50 K above the macroscopic Curie temperature.

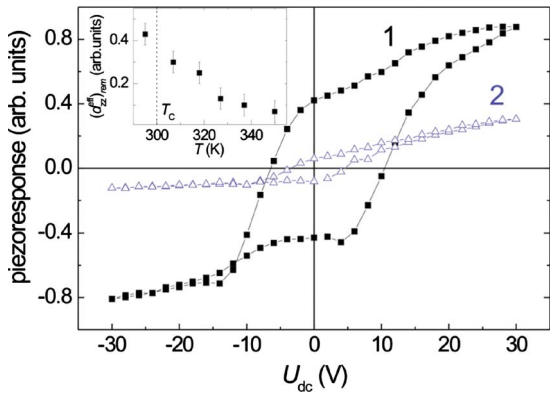

FIG. 6. (Color online) Local piezoresponse hysteresis loops measured on a SBN75 single crystal at 295 (1) and 350 K (2). The inset shows the temperature dependence of the remnant piezoresponse, $(d_{zz}^{eff})_{rem}$ vs T.

We explain this phenomenon as a coalescence of dynamic PNR into larger static entities, which live long enough to be detectable after the removal of the electric field. Since no piezoactive regions were observed after scanning of the treated area, we can estimate the relaxation time for this field-induced piezoactivity to be shorter than about 10^3 s.

IV. CONCLUSIONS

Polar structures of the $Sr_xBa_{1-x}Nb_2O_6$ single crystals were studied by PFM. For ferroelectric SBN at $x=0.4$ we confirm the strong shape anisotropy of domain structure. The structural disorder gives rise to a complexity of patterns containing domains with submicron lateral diameters. This fact points out that SBN compositions with small Sr/Ba ratio differ from conventional ferroelectrics and may be related to a RFIM system with weak RFs. They pin and distort domain walls to form a metastable pattern even after an aging time of one year at room temperature. The polar disorder is enhanced in compositions with higher Sr^{2+} content, which increasingly reveal relaxor behavior. The statistics of the domain sizes and the fractality of their wall contours corroborate theoretical predictions of RFIM systems. The obtained results indicate a strengthening of the RFs at increasing Sr content. In SBN61 and SBN75 large quasistatic PNRs, which are precursors of the domains, are observed above the nominal Curie temperature. At even higher temperatures relatively long-lived polar states may be induced by an external electric field. These results agree with observations obtained in other relaxor systems and evidence the gradual transformation from a ferroelectric into the high-temperature ergodic relaxor state.

ACKNOWLEDGMENTS

Financial support by the European Community within the STREP NMP3-CT-2006-032616 (MULTICERAL) and by KBN (Grant No. 4 T08A 007 25) is gratefully acknowledged.

*vladimir@kleemann.uni-duisburg.de

[1] Y. Xu, *Ferroelectric Materials and Their Applications* (North-Holland, Amsterdam, 1991).
[2] M. H. Francombe, Acta Crystallogr. **13**, 131 (1960).
[3] J. R. Oliver, R. R. Neurgaonkar, and L. E. Cross, J. Appl. Phys. **64**, 37 (1988).
[4] E. Buixaderas, M. Savinov, M. Kempa, S. Veljko, S. Kamba, J. Petzelt, R. Pankrath, and S. Kapphan, J. Phys.: Condens. Matter **17**, 653 (2005).
[5] W. Kleemann, J. Dec, P. Lehnen, R. Blinc, B. Zalar, and R. Pankrath, Europhys. Lett. **57**, 14 (2002).
[6] S. David, T. Granzow, A. Tunyagi, M. Wöhlecke, T. Woike, K. Betzler, M. Ulex, M. Imlau, and R. Pankrath, Phys. Status Solidi A **201**, R49 (2004).
[7] W. Kleemann, J. Mater. Sci. **41**, 129 (2006).
[8] P. Lehnen, W. Kleemann, Th. Woike, and R. Pankrath, Eur. Phys. J. B **14**, 633 (2000).
[9] L. Bursill and P. Lin, Philos. Mag. B **54**, 157 (1987).
[10] D. Viehland, Z. Hu, and W.-H. Huang, Philos. Mag. A **71**, 205 (1995).
[11] A. R. Tunyagi, M. Ulex, and K. Betzler, Phys. Rev. Lett. **90**, 243901 (2003).
[12] U. Voelker and K. Betzler, Phys. Rev. B **74**, 132104 (2006).
[13] J. Dec, W. Kleemann, S. Miga, V. V. Shvartsman, T. Łukasiewicz, and M. Swirkowicz, Phase Transitions **80**, 131 (2007).
[14] P. Lehnen, W. Kleemann, Th. Woike, and R. Pankrath, Phys. Rev. B **64**, 224109 (2001).
[15] W. Kleemann, J. Dec, V. Shvartsman, Z. Kutnjak, and Th. Braun, Phys. Rev. Lett. **97**, 065702 (2006).
[16] J. Dec, V. V. Shvartsman, and W. Kleemann, Appl. Phys. Lett. **89**, 212901 (2006).
[17] V. V. Shvartsman and W. Kleemann, IEEE Trans. Ultrason. Ferroelectr. Freq. Control **53**, 2275 (2006).
[18] T. Łukasiewicz, M. A. Swirkowicz, J. Dec, W. Hofman, and W. Szyrski, J. Cryst. Growth (to be published).
[19] S. V. Kalinin, A. Rar, and S. Jesse, IEEE Trans. Ultrason. Ferroelectr. Freq. Control **53**, 2226 (2006).
[20] M. E. Lines and A. M. Glass, *Principles and Applications of Ferroelectrics and Related Materials* (Clarendon, Oxford, 1979).
[21] U. Nowak, J. Esser, and K. D. Usadel, Physica A **232**, 40 (1996).
[22] J. Esser, U. Nowak, and K. D. Usadel, Phys. Rev. B **55**, 5866 (1997).
[23] J. L. Cambier and M. Nauenberg, Phys. Rev. B **34**, 7998 (1986).
[24] J. Feder, *Fractals* (Plenum, New York, 1988).
[25] V. Likodimos, X. K. Orlik, L. Pardi, M. Labardi, and M. Allegrini, J. Appl. Phys. **87**, 443 (2000).
[26] P. B. Jamieson, S. C. Abrahams, and J. L. Bernstein, J. Chem. Phys. **48**, 5048 (1968).
[27] A. E. Andreichuk, L. M. Dorozhkin, Yu. S. Kuz'minov, I. A. Maslyatsyn, V. N. Molchanov, A. A. Rusakov, V. I. Simonov, V. D. Shigorin, and G. P. Shipulo, Kristallografiya **20**, 1094

(1984).
[28] T. S. Chernaya, B. A. Maksimov, I. V. Verin, L. I. Ivleva, and V. I. Simonov, Crystallogr. Rep. **42**, 375 (1997); J. Schefer, D. Schaniel, V. Pomjakushin, U. Stuhr, V. Petricek, Th. Woike, M. Wöhlecke, and M. Imlau, Phys. Rev. B **74**, 134103 (2006).
[29] C. Laulhé, F. Hippert, J. Kreisel, M. Maglione, A. Simon, J. L. Hazemann, and V. Nassif, Phys. Rev. B **74**, 014106 (2006).
[30] M.-S. Kim, P. Wang, J.-H. Lee, J.-J. Kim, H. Y. Lee, and S.-H. Cho, Jpn. J. Appl. Phys., Part 1 **41**, 7042 (2002).
[31] S. Fishman and A. Aharony, J. Phys. C **12**, L729 (1979).
[32] V. V. Shvartsman, W. Kleemann, J. Dec, Z. K. Xu, and S. G. Lu, J. Appl. Phys. **99**, 124111 (2006).
[33] J. Dec, W. Kleemann, and T. Łukasiewicz, Phase Transitions **79**, 505 (2006).
[34] S. B. Vakhrushev, A. A. Naberezhnov, B. Dkhil, J.-M. Kiat, V. Shvartsman, A. Kholkin, B. Dorner, and A. Ivanov, AIP Conf. Proc. **67**, 74 (2003).
[35] V. V. Shvartsman and A. L. Kholkin, J. Appl. Phys. **101**, 064108 (2007).